Sulfonated poly(diphenylamine) as a novel hole-collecting layer in polymer photovoltaic cells. J Mater Chem

ARTICLE *in* JOURNAL OF MATERIALS CHEMISTRY · JANUARY 2008

Impact Factor: 7.44 · DOI: 10.1039/b807182a

3 AUTHORS, INCLUDING:

Ten-Chin Wen
National Cheng Kung University
275 PUBLICATIONS **5,438** CITATIONS

Sulfonated poly(diphenylamine) as a novel hole-collecting layer in polymer photovoltaic cells

Chen-Yan Li,[a] Ten-Chin Wen*[a] and Tzung-Fang Guo*[b]

Received 28th April 2008, Accepted 3rd July 2008
First published as an Advance Article on the web 13th August 2008
DOI: 10.1039/b807182a

Sulfonated poly(diphenylamine) (SPDPA) was used as a novel hole-collecting layer (HCL) in polymer photovoltaic (PV) cells. PV cells of poly(3-hexylthiophene) (P3HT):[6,6]-phenyl C_{61} butyric acid methyl ester used as the active layer with SPDPA as HCL showed the higher power conversion efficiency (4.2%) and fill factor (0.68) than those with commercial poly(3,4-ethylenedioxythiophene): poly(styrenesulfonate) (Baytron AI 4083) (3.6% and 0.65). The morphology change of the active layer was observed using atomic force microscopy and grazing-incidence X-ray diffraction. The hole-only device was fabricated to measure hole-injection current and hole mobility. The results show increased crystallinity of P3HT with SPDPA as HCL. The enhanced device performance is attributed to the improved hole mobility and the increased crystallinity of P3HT due to the properties of SPDPA.

Introduction

Polymer photovoltaic (PV) cells have tremendous potential as renewable, alternative sources of energy because they are flexible, light-weight, and inexpensive. The poly(3-hexylthiophene) (P3HT) and [6,6]-phenyl C_{61} butyric acid methyl ester (PCBM) blending system has made great progress. The power conversion efficiency (PCE) has been enhanced to 4–5% through treatments such as thermally annealing,[1,2] slow drying,[3] and adding a surfactant into active layer,[4] which increase polymer crystallinity. High PCEs of more than 6% were achieved by fabricating a tandem cell architecture, where two devices with different absorption characteristics are linked to utilize a wider range of the solar spectrum.[5]

Besides controlling the morphology of polymer composites, PCE could be raised by applying appropriate electrodes. For example, LiF/Al[6] or Ca/Al[7] can be used as the electron-collecting layer to improve the open-circuit voltage (V_{oc}) and fill-factor (FF) of PV cells. The LUMO levels of the acceptor pin the Fermi levels of the contact electrode, which results in the band bending and the interfacial barrier resistance being reduced. Recently, it was reported that polymeric material poly(ethylene oxide) as used the electron-collecting electrode was able to increase V_{oc} in PV cells.[8]

Commercial poly(3,4-ethylenedioxythiophene):poly(styrene sulfonate) (PEDOT: PSS) has always been used as a hole-collecting layer (HCL). Ko *et al.* improved the conductivity of PEDOT:PSS by utilizing mannitol.[9] Enhanced short-circuit current density (J_{sc}) and PCE could be observed due to a reduction of the series resistance (R_s). Related studies indicated that the buffer layers in organic or polymer electronic devices played a significant role in controlling the carrier transport or collection. Besides, HCL may influence the arrangement of the active layer due to its interfacial interaction. In the case of organic field-effect transistors, the molecular orientation of P3HT was controlled by various functional groups of self-assembled monolayers due to the difference of intermolecular interaction between P3HT and substrate.[10] The different surface treatment, converting the hydrophilic surface to hydrophobic surface, would probably improve the surface roughness, orientation, and crystallinity of P3HT films.

In this study, we report a novel hole-collecting layer, sulfonated poly(diphenylamine) (SPDPA), with high transmittance (near 80% transmittance in visible region) and an appropriate work function (~5.24 eV). Due to its chemical structure, polarity, and the surface energy, the SPDPA increases the crystallinity of P3HT in the active layer during the spin-coating and film-growing processes, resulting in enhanced PCE.

Experimental

The novel HCL, SPDPA, was synthesized using oxidative polymerization coupled with a facile sulfonation process. The details of the preparation procedure and characterization can be found in our previous work.[11] Commercial PEDOT:PSS (Baytron-P AI 4083) was utilized as HCL for comparison. The chemical structures of SPDPA and PEDOT:PSS are shown in Fig. 1.

PV cells were fabricated by coating the active layer of P3HT:PCBM, which was sandwiched between the hole-collecting electrode, a transparent ITO (received from RITEK Corp., 15 Ω $\square^{-1}$)/HCL, and the electron-collecting electrode, calcium (Ca) (40 nm)/aluminium (Al) (100 nm). In the hole-only device, gold (Au) (30 nm) and silver (Ag) (100 nm) were thermally deposited onto the P3HT:PCBM film as the top electrode. The active area of the device was 0.08 cm^2. Before device fabrication, the ITO glass substrates were sequentially cleaned by ultrasonic treatment in detergent, deionized water, acetone, and isopropyl

[a]*Department of Chemical Engineering, Advanced Optoelectronic Technology Center, National Cheng Kung University, Tainan 70101, Taiwan. E-mail: tcwen@mail.ncku.edu.tw*
[b]*Institute of Electro-Optical Science and Engineering, Advanced Optoelectronic Technology Center, National Cheng Kung University, Tainan 70101, Taiwan. E-mail: guotf@mail.ncku.edu.tw*

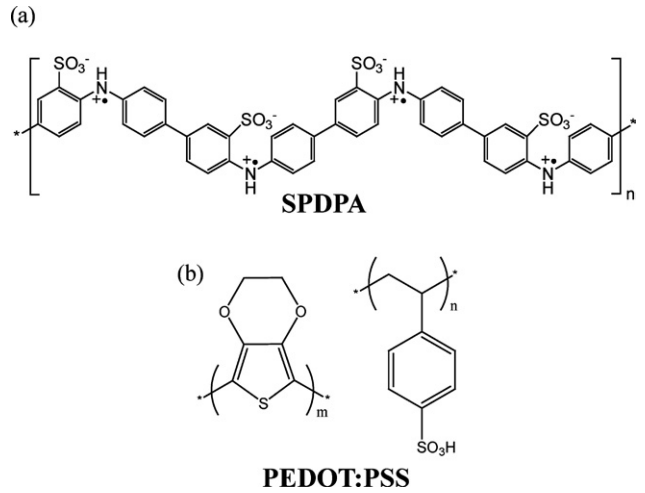

Fig. 1 The molecular structures of the hole-collecting layer for this work.

alcohol. The hole-collection layers of PEDOT:PSS and SPDPA (concentration of 1.2 wt.% in deionized water) were spin-coated to modify the ITO surface. After baking at 150 °C for 30 min, the substrates were transferred to a nitrogen-filled glove box. P3HT (Nano-c) and PCBM (Nano-c) had a ratio of 1 : 1 with a concentration of 2 wt.% in 1,2-dichlorobenzene. The blend was stirred for at least 24 h at room temperature in the glove box. The active layer was spin-coated at 650 rpm for 60 s and then transferred to a sealed glass petri dish to carry out the solvent-annealing procedure as described in ref. 3 (denoted as slow-grown film). The fast-grown film was spin-coated at 1200 rpm for 60 s, and its surface morphology was investigated using atomic force microscopy (AFM). In order to avoid morphological changes upon heat annealing, the devices did not undergo any baking treatment. The current density–voltage (J–V) characteristics of the devices were measured with a Keithley 2400 source-measure unit under simulated AM 1.5 G irradiation (100 mW cm^{-2}) using an Oriel 91160A 300 W Solar Simulator in the glove box. The illumination intensity used was calibrated by a standard Si photodiode detector with a KG-5 color filter (Hamamastsu, S1133).[12] The incident photon-to-electron conversion efficiency (IPCE) spectra were measured with a lock-in pre-amplifier (SR510, Standard Research Systems) after the devices were illuminated with monochromatic light using a xenon lamp (Oriel 66902 150 mW Solar Simulator) passing through a monochromator (Oriel Cornerstone 130™ 1/8 m monochromator). The spectral response was normalized by a standard mono-silicon solar cell before the IPCE data was taken.

The surface energies of PEDOT:PSS and SPDPA were determined using Owens–Wendt contact angle measurements with water and diiodomethane as probe liquids.[13] The work functions were measured using a Riken Keiki AC-2 photoelectron spectroscope in air. Conductivity was measured using a four-point probe experiment. Transmittance spectra were analyzed with a UV-visible spectrometer constructed by GBC Scientific Equipment, Australia (model GBC Cintra 10 e). AFM was performed with a NanoScope IIIa (Digital Instruments Inc.) run in the tapping mode. The synchrotron grazing-incidence X-ray diffraction (GI-XRD) measurements were performed at the 17B1 beamline (wavelength $\sim$ 1.37 Å) of National Synchrotron Radiation Research Center in Taiwan. The grazing incidence angle was fixed at 0.18°. The thickness measurements were made using a Tencor Alpha-Step 500 Surface profiler.

Results

The device performance of PV cells depended on J_{sc}, V_{oc}, and FF. These parameters are directly determined by overall device resistance, including intrinsic conductivity of the collecting layer, barrier height at the interface, and the carrier mobility of the active layer. The corresponding data of polymeric characteristics are listed in Table 1. The work function of SPDPA (5.24 eV) and PEDOT:PSS (5.07 eV) is higher than the HOMO of P3HT (4.9 eV). This implies that both cases can avoid having an unnecessary interfacial barrier. The morphology of active layer can be affected by the surface energy and polarity of the bottom layer upon annealing,[14,15] so the contact angle and surface energy experiments were conducted. The small contact angle and high surface energy of SPDPA are attributable to its hydrophilic property due to NH and SO_3H groups (one SO_3H group attached to every phenyl ring) on its polymer chain. High conductivity of HCL is an important factor in avoiding a transporting bottleneck in the hole-collecting electrode. Unfortunately, SPDPA has a lower conductivity than PEDOT:PSS. To overcome this, the thickness of the SPDPA layer can be reduced for optimal resistance.

Fig. 2(a) and 1(b) show the current density–voltage (J–V) behaviour of PV cells under illumination and dark, respectively. In the dark, the same order of magnitude is achieved for leakage current and rectification of PV cells based on PEDOT:PSS and SPDPA with various thicknesses. This indicates that both SPDPA and PEDOT:PSS provide good modification and buffer functions. The thickness of SPDPA was controlled at about 26 nm, 14 nm, and 10 nm using spin-coating rates of 1500, 3500 and 5500 rpm, respectively. Under illumination, all PV cells had almost the same V_{oc} (0.60 V), which can be attributed to the Ohmic contact effect between P3HT and HCLs, as reported by

Table 1 Polymeric surface characteristics and roughness for PEDOT:PSS and SPDPA as hole-collecting layers

			Contact angle/°			
Material	Work function[a]/eV	Conductivity[b]/S cm^{-1}	Water	Diiodomethane	Surface energy/mJ m^{-2}	Surface roughness/nm
PEDOT	5.07	8.3×10^{-4}	21.6	29.4	68.5	0.94
SPDPA	5.24	1.1×10^{-4}	<10	19.8	72.7	0.91

[a] Measured using the AC-2 photoelectron spectroscope. [b] Measured using the four-point probe.

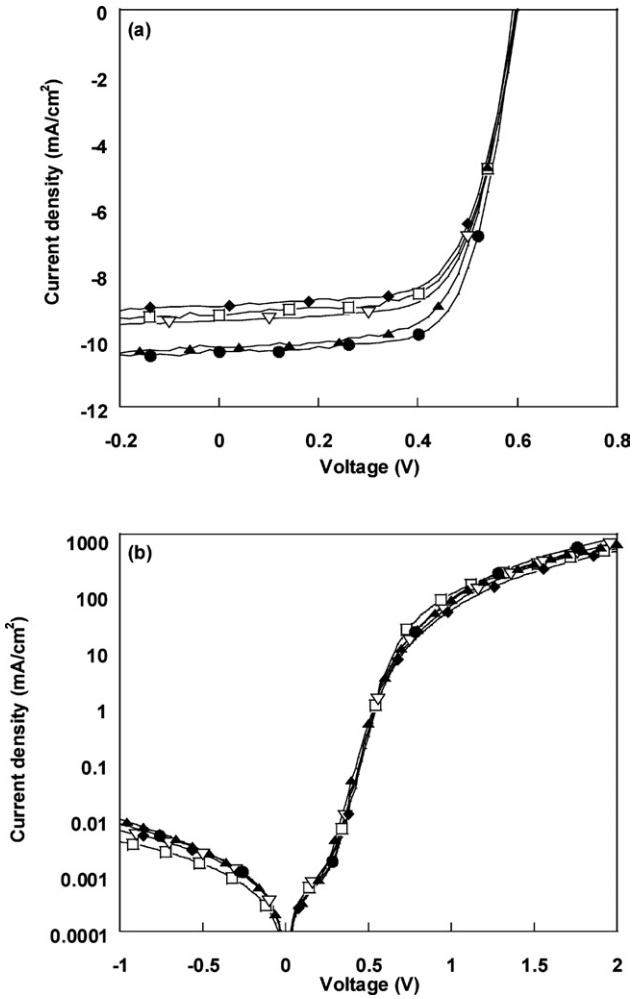

Fig. 2 *J–V* curves of PV cells based on P3HT:PCBM with (□) 30 nm PEDOT:PSS, (▽) 10 nm PEDOT:PSS, (◆) 26 nm SPDPA, (▲) 14 nm SPDPA and (●) 10 nm SPDPA (a) under AM 1.5 (100 mW cm^{-2}) illumination and (b) under dark.

Mihailetchi *et al.*[7] In our case, V_{oc} is determined using the molecular energy difference between the donor HOMO and the acceptor LUMO. For convenience, all performance parameters derived from Fig. 1 are listed in Table 2. Surprisingly, both J_{sc} and PCE progressively increase with decreasing SPDPA thickness. The device based on SPDPA (10 nm) can achieve 4.2% PCE, which exceeds the 3.6% of the device based on PEDOT:PSS. On the contrary, less J_{sc} was collected from the device based on 26 nm SPDPA than that from PEDOT:PSS, which can be attributed to the lower conductivity of SPDPA. For a fair comparison, devices based on 10 nm PEDOT:PSS were also fabricated; the corresponding data was summarized in Table 2. Although the thickness of PEDOT:PSS was reduced to avoid hole-transporting obstruction, the device performance was not significantly enhanced. The series resistance (R_s), including the resistance of the active layer, metal–organic contacts, and collecting electrode represents the Ohmic loss, which significantly affects device performance.[9] Here, R_s was calculated from *J–V* curves in the dark (Fig. 2(b)). R_s also decreases with decreasing SPDPA thickness. The R_s of the device based on 10 nm SPDPA is much smaller than that of the devices based on PEDOT:PSS (both 10 and 30 nm PEDOT:PSS), which is favourable for charge transporting. FF increased to 0.68 when thickness decreased to 10 nm, implying that the electron–hole pairs are more equally separated and transported to the collecting electrodes in this case. In the P3HT:PCBM device, hole mobility is smaller than electron mobility. An improvement in hole mobility balances the separation efficiency and consequently reduces the space-charge effect. The above results are consistent with increased FF. It seems that 10 nm SPDPA as HCL improves FF and hole mobility.

The IPCE and transmittance spectra of HCL were measured, as shown in Fig. 3. Both PEDOT:PSS and SPDPA coated on ITO have about 86% transmittance between 450 nm and 750 nm wavelengths. SPDPA has the stronger absorption in the range of 350 nm to 450 nm than PEDOT:PSS does due to the π–π* transition of the benziod ring. IPCE spectra of devices based on PEDOT:PSS and SPDPA show similar curves, although the

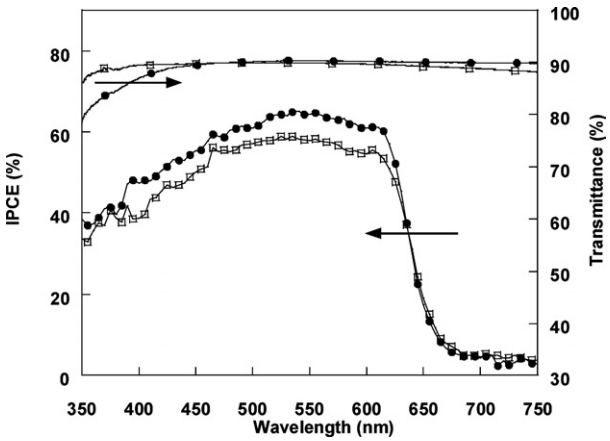

Fig. 3 IPCE spectra for PV cells with PEDOT:PSS (□) and SPDPA (●); transmittance spectra of PEDOT:PSS (□) and SPDPA coated on ITO (●).

Table 2 The device performance of various hole-collecting layers

Material	V_{oc}/V	J_{sc}/mA cm^{-2}	FF	PCE (%)	R_s[a]/Ω cm^2
PEDOT 4000 rpm (30 nm)	0.60	9.23	0.65	3.6	3.03
PEDOT 8000 rpm (10 nm)	0.60	9.39	0.66	3.7	2.35
SPDPA 1500 rpm (26 nm)	0.60	8.96	0.65	3.5	3.31
SPDPA 3500 rpm (14 nm)	0.58	10.21	0.66	3.9	2.47
SPDPA 5500 rpm (10 nm)	0.60	10.33	0.68	4.2	1.93

[a] Calculated using the *J–V* curves in the dark.

slightly lower transmittance of SPDPA in this region could consume some incident photons. The maximum IPCE reaches about 65.2% and 58.8% for devices based on 10 nm SPDPA and PEDOT:PSS, respectively. This is consistent with J_{sc} data under AM 1.5 G illumination.

It is interesting that the device based on 10nm SPDPA had a 4.2% PCE with a high FF value of 0.68, being attributable to the higher hole-transporting property of SPDPA devices than PEDOT:PSS devices. Related studies indicated that interfacial interactions could influence molecular arrangement upon casting film.[10,16] Fig. 4 shows atomic force microscopy (AFM) height images of P3HT:PCBM coated on PEDOT:PSS and SPDPA *via* the solvent-annealing process. A very thin film was also prepared by spin-coating at 1200 rpm to observe the morphology of the active layer near HCL (denoted as fast-grown film). The surface roughness of SPDPA and PEDOT:PSS coated on ITO was ascertained to be the same (Table 1). For P3HT:PCBM film on PEDOT:PSS, the root mean square (rms) roughness values of fast-grown film and slow-grown film were 1.12 nm and 8.07 nm, respectively. The surface roughness becomes bigger after the solvent-annealing process due to polymer self-organization. Similarly, a rougher surface was observed in slow-grown film (rms $\sim$ 12.61 nm) than that in fast-grown film (rms $\sim$ 1.78 nm) for P3HT:PCBM on SPDPA. The surface roughness was larger on SPDPA than on PEDOT:PSS. Regarding coarse surface roughness, some reports have considered the existence of an interfacial area for charge separation[1] or high crystallinity within two phase networks.[4]

While AFM images are useful for identifying the surface morphology of films, they cannot be used to determine the structure of the active layer. Therefore, the synchrotron grazing-incidence X-ray diffraction (GI-XRD) measurement was employed to reveal the film structure. Here, the grazing incidence was fixed at a very small angle in order to conduct the measurements at the same thicknesses. Fig. 5 shows XRD patterns for the crystalline structures of P3HT:PCBM films on both PEDOT and SPDPA substrates. The high intensities found for both (100) and (200) reflection peaks belong to P3HT with prevailing *a*-axis orientation, indicating that the main (side) chain is parallel (perpendicular) to the substrate. We also found that the film structure on SPDPA appears more ordered than that on PEDOT:PSS, which can be explained as follows. For a pure P3HT film, specially on a substrate having strong polar groups, P3HT tends to be repelled by the polar groups due to the

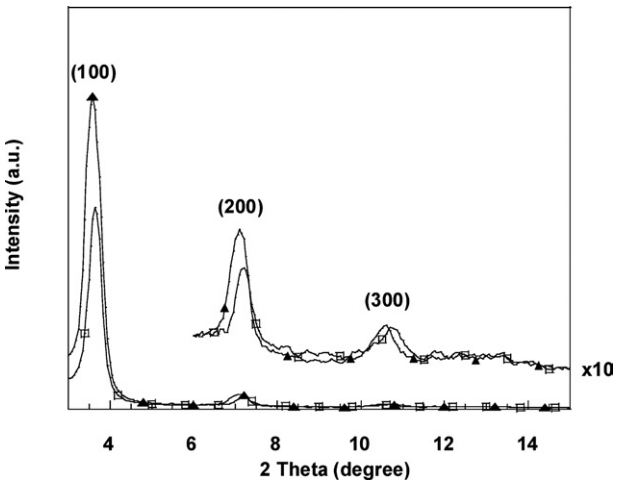

Fig. 5 GI-XRD spectra of P3HT:PCBM slow-grown film onto ITO/PEDOT:PSS (□) and ITO/SPDPA (▲) substrates.

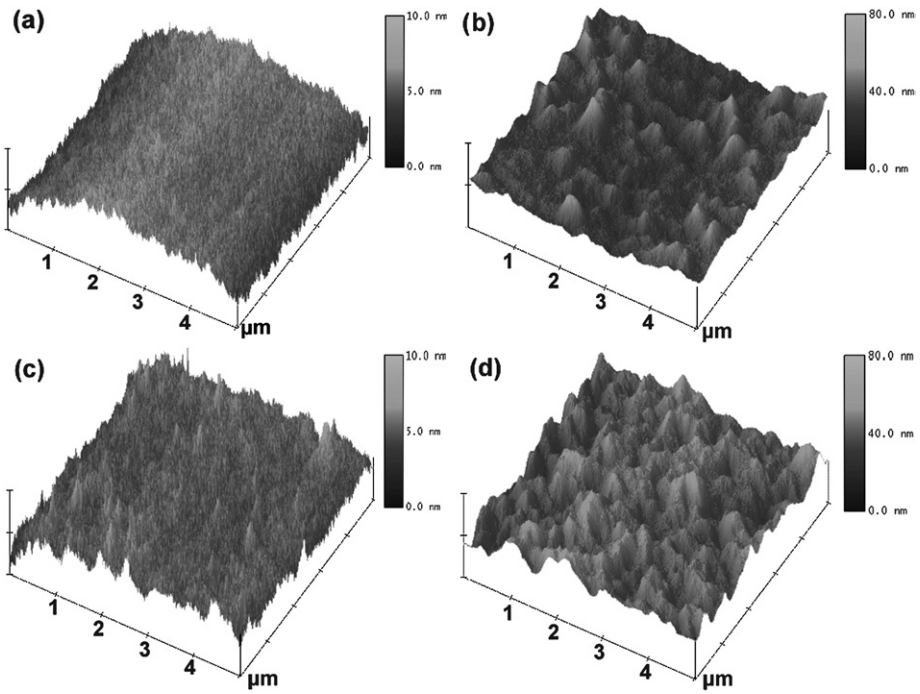

Fig. 4 AFM images of P3HT:PCBM deposited on (a) PEDOT:PSS *via* fast-grown film; (b) PEDOT:PSS *via* slow-grown film; (c) SPDPA *via* fast-grown film; (d) SPDPA *via* slow-grown film.

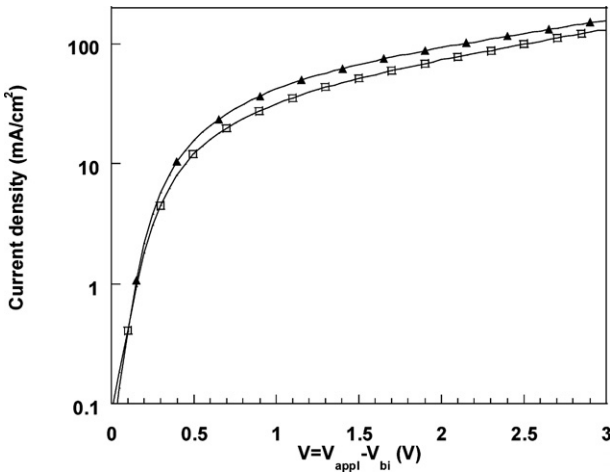

Fig. 6 *J–V* curves for hole-only devices based on P3HT:PCBM slow-grown film with various hole-collecting layers: PEDOT (□) and SPDPA at 3500 rpm (▲). We corrected the applied voltage (V_{appl}) with a build-in voltage (V_{bi}). The V_{bi} value is 0.1 V. The thicknesses of polymer films, including the HCL layer and active layer, are 220 nm for PEDOT:PSS and 206 nm for SPDPA.

overlap of their electron clouds so the assembled P3HT molecules are inclined to lay on the substrate with their side chains in the orientation perpendicular to the substrate.[10] Earlier reports indicated that P3HT with PCBM can exhibit a more evident molecular orientation in the *a*-axis direction.[14] Together with the fact that SPDPA has a strong polarity and can assist P3HT:PCBM molecules in the *a*-axis orientation, P3HT:PCBM assembly near the interface is guided by SPDPA, forming a more ordered structure. As these assembled molecules pile up layer-by-layer, they become susceptible to being self-organized into a highly ordered lamellar structure. The performance of the whole active layer can be enhanced by increased crystallinity.

From the above discussion of roughness and crystallinity of P3HT on SPDPA, we presume that the hole mobility is enhanced. In order to validate this presumption, we fabricated hole-only devices with the following structure: ITO/HCL/P3HT:PCBM/Au/Ag. The *J–V* curves of the hole-only devices are shown in Fig. 6. Here, we correct voltage (V_{appl}) with build-in potential (V_{bi}) using $V = V_{appl} - V_{bi}$. The device based on SPDPA exhibits more current density than that based on PEDOT:PSS at the same operating voltage, confirming the enhancement of hole mobility by SPDPA. The curves were fitted using the SCLC model at a low bias to calculate hole mobility.[17] The calculation used $J = 9\varepsilon_0\varepsilon_r\mu V^2/8L^3$, where $\varepsilon_0\varepsilon_r$ is the permittivity of the polymer, μ is the carrier mobility, and L is the device thickness. A higher hole mobility can be calculated in the device based on SPDPA (1.55×10^{-7} m^2 V^{-1} s^{-1}), as compared to that based on PEDOT:PSS (1.36×10^{-7} m^2 V^{-1} s^{-1}). This result confirms that the high PCE of the device based on 10 nm SPDPA is attributed to the increased crystallinity of P3HT and enhanced hole mobility.

Conclusion

We have a successful demonstration using SPDPA as HCL in polymer PV cells. Excellent device performances including 4.2% PCE, 0.68 FF, and 65.2% IPCE are obtained for the device based on 10 nm SPDPA as HCL. The role of 10 nm SPDPA is used to obtain high crystallinity of P3HT, to enhance the hole mobility, to reduce the series resistance, and to produce an Ohmic contact between HCL and P3HT. We hope that this demonstration will stimulate more studies on polymer PV cells with the inverted structure because SPDPA can be well dissolved in other organic polar solvents.

Acknowledgements

This research was supported by the National Science Council of Taiwan under NSC-96-2221-E-006–059, NSC-95-2111-E-006-409-MY3, and Asian Office of Aerospace Research and Development (AOARD-07-4068). We would like to thank Mr Ching-Chang Tseng from Chi Mei EL Corporation for measuring the work functions of polymeric materials. The authors would also like to thank Prof. Hsien-Hung Wei for his help in GI-XRD analyses as well as Mr Tsung-Hsun Lee for his help in GI-XRD measurements.

References

1 W. L. Ma, C. Y. Yang, X. Gong, K. Lee and A. J. Heeger, *Adv. Funct. Mater.*, 2005, **15**, 1617.
2 M. Reyes-Reyes, K. Kim and D. L. Carroll, *Appl. Phys. Lett.*, 2005, **87**, 083506.
3 G. Li, V. Shrotriya, J. S. Huang, Y. Yao, T. Moriarty, K. Emery and Y. Yang, *Nat. Mater.*, 2005, **4**, 864.
4 W. Wang, H. B. Wu, C. Y. Yang, C. Luo, Y. Zhang, J. W. Chen and Y. Cao, *Appl. Phys. Lett.*, 2007, **90**, 183512.
5 J. Y. Kim, K. H. Lee, N. E. Coates, D. Moses, T. Q. Nguyen, M. Dante and A. J. Heeger, *Science*, 2007, **317**, 222.
6 C. J. Brabec, S. E. Shaheen, C. Winder, S. Sariciftci and P. Denk, *Appl. Phys. Lett.*, 2002, **80**, 1288.
7 V. D. Mihailetchi, P. W. M. Blom, J. C. Hummeien and M. T. Rispens, *J. Appl. Phys.*, 2003, **94**, 6849.
8 F. Zhang, M. Ceder and O. Inganas, *Adv. Mater.*, 2007, **19**, 1835.
9 C. J. Ko, Y. K. Lin, F. C. Chen and C. W. Chu, *Appl. Phys. Lett.*, 2007, **90**, 063509.
10 D. H. Kim, Y. D. Park, Y. Jang, H. Y, Y. H. Kim, J. I. Han, D. G. Moon, S. Park, T. Chuang, C. Chang, M. Joo and C. Y. Ryu, *Adv. Funct. Mater.*, 2005, **15**, 77.
11 C. Y. Li, T. C. Wen, T. F. Guo and S. S. Hou, *Polymer*, 2008, **49**, 957.
12 V. Shrotriya, G. Li, Y. Yao, T. Moriarty, K. Emery and Y. Yang, *Adv. Funct. Mater.*, 2006, **16**, 2016.
13 M. Zenkiewicz, *Polym. Test.*, 2007, **26**, 14.
14 J. S. Kim, J. H. Park, J. H. Lee, J. Jo, D. Y. Kim and K. Cho, *Appl. Phys. Lett.*, 2007, **91**, 112111.
15 M. Campoy-Quiles, T. Ferenczi, T. Agostinelli, P. G. Etchegoin, Y. K. Kim, T. D. Anthopoulos, P. N. Stavrinou, D. D. C. Bradley and J. Nelson, *Nat. Mater.*, 2007, **7**, 158.
16 R. J. Kline, M. D. Mcgehee and M. F. Toney, *Nat. Mater.*, 2006, **5**, 222.
17 V. Shrotriya, Y. Yao, G. Li and Y. Yang, *Appl. Phys. Lett.*, 2006, **89**, 063505.

